

Trade-offs in Analog Sensing and Communication in RF Energy Harvesting Wireless Sensor Networks

M. P. Praveen

Neelesh B. Mehta, *Senior Member, IEEE*

Abstract—Radio-frequency (RF) energy harvesting (EH) is an appealing solution for making wireless sensor networks (WSNs) self-reliant in terms of energy. We investigate the problem of sensing and estimation in a WSN for a practically motivated transmit and receive model. In it, noisy readings are communicated by multiple peak-power constrained RF EH sensor nodes in an analog manner using phase modulation to a fusion node, which uses the popular phase-locked loop (PLL) circuit for signal reception. For the time-sharing model, in which an EH sensor node alternately harvests energy and transmits data, and for a general class of stationary and ergodic RF EH processes, we present insightful expressions for the mean squared error (MSE) of the estimate at the fusion node, and optimal fraction of time a node harvests energy and optimal transmit power that minimize the MSE. Benchmarking with several digital schemes brings out the natural adaptability and efficacy of the considered scheme.

I. INTRODUCTION

Energy harvesting (EH) is a promising solution for improving the lifetime of wireless sensor networks (WSNs) and making them self-reliant. In it, each node harvests renewable energy from its environment, and stores it in a battery or super-capacitor. It uses this energy to transmit its measured data over a wireless channel to a fusion node [1]–[3].

Given its promise, estimation with EH sensor nodes, in which the sensor nodes measure a parameter and communicate their measurements over wireless links to a fusion node, which then estimates it, is attracting increasing attention in the literature. In a WSN consisting of EH nodes, the transmit power of the sensor nodes is optimized to minimize the mean squared error (MSE) of the estimate at the fusion node for a finite number of estimation periods with a best linear unbiased estimator in [2]. The energy harvested in each slot and the channel gains between the sensor nodes and fusion node in each slot are assumed to be known a priori. Optimal power allocation strategies that minimize the MSE of the estimate at the fusion node, which uses a minimum mean squared error (MMSE) estimator, are studied in [1] for an additive white Gaussian noise channel. In [4], a maximum-likelihood estimator is studied instead. Optimal energy allocation policies for Markovian fading channels are studied in [3]. Estimation of the max function in an EH WSN was studied in [5].

The authors are with the Dept. of Electrical Communication Eng. at the Indian Institute of Science (IISc), Bangalore, India. Emails: mp-praveen47@gmail.com, nbmehta@ece.iisc.ernet.in. This work was partially supported by a research grant from the Aerospace Network Research Consortium (ANRC).

A. RF Energy Harvesting WSNs and Their Trade-offs

Radio-frequency (RF) EH is a special case of EH in which the nodes harvest energy from electromagnetic radiations [6]. The source of RF energy may be an RF power source that is dedicated for feeding energy to the nodes [7] or ambient electromagnetic radiations from cellular base stations or WiFi access points [6]. The availability of higher-efficiency circuits and the decrease in power requirements of the sensor nodes have made RF EH practically appealing [8].

Two methods, namely, power splitting and time-sharing, were proposed for decoding data and harvesting energy from the received signal in [9]. A similar issue arises at the transmitter as well. It is studied in [7] in the setting where a multi-antenna access point broadcasts wireless power to single antenna sensor nodes. These, in turn, transmit data to it using the time-sharing model, in which an EH node alternates between EH and transmission.

Simultaneous RF EH and data transfer can also be done by having different antennas dedicated for transmission and EH [10]. However, in small sensor nodes, such as wearables, integrating more than one antenna into the node can be challenging and expensive. For such devices, time-sharing is of practical interest, and is the focus of our paper.

B. Contributions

Since both energy harvesting and communication processes involve electromagnetic radiations and a practical RF EH circuit cannot simultaneously decode the data present in the signal [9], new trade-offs arise in the design of RF EH WSNs [11]. For a WSN in which multiple RF EH sensor nodes measure a parameter, and communicate their noisy measurements to a fusion node over a wireless fading channel in an analog manner using phase modulation, we highlight, analyze, and optimize these trade-offs. The fusion node employs the widely used phase-locked loop (PLL) circuit for decoding the phase information sent from the sensor node, and thereafter computes the MMSE estimate of the parameter.

For the time-sharing model and a Gaussian distributed parameter and noise model, we optimize the fading-averaged MSE of the estimate at the fusion node as a function of the fraction τ of time energy is harvested by a sensor node in a slot. Firstly, we characterize the trade-off involved in choosing the transmit duration, which affects the accuracy of the readings transmitted by the EH node and the rate at which it harvests energy for these transmissions. Secondly, we study the trade-off involved in setting the transmit power,

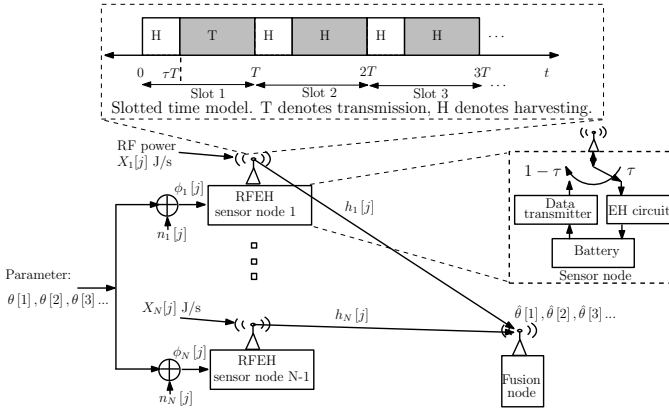


Fig. 1. System model consisting of RF EH sensor nodes and a fusion node. Also shown are the transmission and EH models.

which also affects the accuracy of the readings transmitted and the subsequent evolution of the node's battery energy.

Our model differs from [12] in its use of non-quantized analog transmission and from [1]–[4] in its use of phase-based modulation and PLL-based estimation at the receiver. Our approach is novel and relevant for the following reasons. Firstly, we focus on analog transmission because it can outperform coding schemes designed according to the source-channel separation principle in sensing applications [13]. Secondly, embedding the measurement in phase ensures a fixed transmit power, which enables the use of efficient transmit power amplifiers at the sensor nodes. Practical limitations on power amplifiers also motivate our modeling of a peak transmit power constraint. Thirdly, we model, analyze, and simulate the use of a PLL circuit at the receiver, which is widely used in practical designs. Fourthly, we present benchmarking results that demonstrate the efficacy and robustness of the analog scheme compared to digital schemes that employ quantization followed by digital transmission of the measurement. We show that the analog sensing and communication scheme possesses a natural adaptability to parameters such as signal-to-noise ratio (SNR) and τ , unlike its digital counterparts.

C. Outline

Section II describes the system model. In Section III, we analyze and optimize the MSE of the estimate. Numerical results are presented in Section IV, and are followed by our conclusions in Section V. Proofs are relegated to the Appendix.

II. SYSTEM MODEL

Consider a WSN that consists of N RF EH sensor nodes and a fusion node, as shown in Figure 1. The time is assumed to be slotted. The slot duration is T seconds. We now explain the EH, measurement, transmission, channel, and receiver models.

RF EH Model: Let $X_i[j]$ denote the rate at which energy is harvested by sensor node i in slot j . It is assumed to be a stationary and ergodic random process with mean $\mathbb{E}[X_i[j]] = P_{\text{eh}}$ J/s, where $\mathbb{E}[\cdot]$ denotes expectation. This general model

encompasses several models studied in the literature such as the Bernoulli and Markovian models [14].

In each slot, for the first τT duration, each RF EH sensor node harvests energy from its environment at an average rate of P_{eh} J/s. Thereafter, each sensor node checks whether its battery energy is sufficient to transmit the sensed measurement for the remaining $(1 - \tau)T$ time in the slot. If the battery energy is sufficient, then the sensor node commences data transmission as described below. Else, it continues to harvest energy from the environment in this duration as well.

Measurement Model: In the j^{th} slot, the sensor node i measures the parameter $\theta[j]$, which is perturbed by a node-specific measurement noise $n_i[j]$. Such a model has also been used in [2], [15]. The noise is modeled as a Gaussian random variable (RV). Thus, the measurement output $\phi_i[j]$ of sensor node i in slot j is

$$\phi_i[j] = \theta[j] + n_i[j], \quad (1)$$

where $n_i[j] \sim \mathcal{N}(0, \sigma_m^2)$ and $\theta[j] \sim \mathcal{N}(0, \sigma_\theta^2)$ [1], [15]. Here, the notation $X \sim \mathcal{N}(\mu, \sigma^2)$ implies that X is a Gaussian RV with mean μ and variance σ^2 . We shall also assume that $n_i[j]$ is i.i.d. across i and j , and is statistically independent of $\theta[j]$.

Transmission Model: As mentioned, a sensor node transmits its measurement using phase modulation, if the energy stored in its battery is sufficient. In such a case, we say that the sensor node is *active*. Else, it is said to be *inactive*. Let $\mathcal{A}[j]$ denote the set of all active nodes in slot j . In slot j , the transmitted signal $x_i(t)$ by node i , for $t \in [(j-1)T + \tau T, jT]$, is

$$x_i(t) = \begin{cases} \sqrt{2P} \cos(2\pi f_{c_i} t + \phi_i[j]), & \text{if } B_i[j] \geq PT(1 - \tau), \\ 0, & \text{if } B_i[j] < PT(1 - \tau), \end{cases} \quad (2)$$

where P is transmit power, $B_i[j]$ denotes the energy stored in the battery of node i at time $(j-1)T + \tau T$, and f_{c_i} is the carrier frequency for transmissions by node i . Thus, $i \in \mathcal{A}[j]$ if $B_i[j] \geq PT(1 - \tau)$. Let P_{max} denote the peak transmit power. The nodes transmit on orthogonal channels.

Note: $\phi_i[j]$ should lie in $[-\pi, \pi)$ to avoid phase ambiguity. If this is not the case, one can scale $\phi_i[j]$ by a factor $\gamma \in (0, 1]$ so that $\gamma\phi_i[j]$ lies in $[-\pi, \pi)$ with high probability. It can be shown that introducing the factor $\gamma < 1$ is equivalent to enhancing the noise power at the receiver by a factor $\frac{1}{\gamma^2}$. For ease of exposition, we set $\gamma = 1$ henceforth.

Channel Model: Let $h_i[j]$ denote the passband channel amplitude from sensor node i to the fusion node in the j^{th} slot. It is a Rayleigh RV with unit mean power. The channels between the sensor nodes and the fusion node are assumed to undergo independent block fading. The received signal $y_i(t)$, for $t \in [(j-1)T + \tau T, jT]$, at the fusion node from sensor node i is given by

$$y_i(t) = h_i[j]x_i(t - \xi_i[j]) + e_i(t), \\ = \begin{cases} \sqrt{2P}h_i[j]\cos(2\pi f_{c_i} t + \Delta_i[j]) + e_i(t), & i \in \mathcal{A}[j], \\ e_i(t), & \text{else,} \end{cases} \quad (3)$$

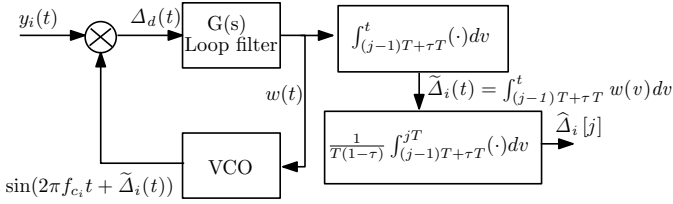


Fig. 2. Receiver structure based on PLL to estimate phase $\hat{\Delta}_i[j]$ in a slot j .

where ξ_i is the time delay introduced by the channel, $e_i(t)$ is white Gaussian noise process with power spectral density $N_0/2$, and $\Delta_i[j] = \phi_i[j] - 2\pi f_{c_i} \xi_i[j]$. We assume that $h_i[j]$ and $\xi_i[j]$ are known at the receiver if the node is active. They can be estimated by the node using pilots.

Receiver Model: The receiver consists of PLL-based phase demodulators to decode the received signals from each of the N sensors, as shown in Fig. 2. If node i is active in slot j , the PLL corresponding to it is turned on and it extracts the phase $\Delta_i[j]$ from the received signal $y_i(t)$.

The PLL consists of a phase detector, a loop filter, and a voltage controlled oscillator (VCO). The phase detector multiplies its two input signals and filters out the high frequency components in the resulting product to give the signal $\Delta_d(t)$ at its output. The VCO generates a sinusoid synchronized in frequency to the received waveform. Its phase $\tilde{\Delta}_i(t)$ is equal to the cumulative error $w(t)$ shifted by $\frac{\pi}{2}$ radians.

The phase estimate $\tilde{\Delta}_i(t) = \int_{(j-1)T+\tau T}^t w(v) dv$ at time t , which is obtained by integrating the signal $w(t)$ input to the VCO, is noisy due to the presence of noise in the signal input to the phase detector. It is, therefore, averaged over the transmission duration $T(1-\tau)$ to get the phase estimate of the received signal as $\hat{\Delta}_i[j]$. The receiver then compensates for the phase shift introduced by the channel by adding the phase $2\pi f_{c_i} \xi_i[j]$ to $\hat{\Delta}_i[j]$ to get the observation $\hat{\phi}_i[j]$. The loop filter $G(s)$ is selected such that the closed-loop transfer function of the PLL $H(s) = \frac{G(s)}{s+G(s)}$ is of second-order [16].

If a sensor node is inactive, then the corresponding PLL is not activated [4]. The state of the sensor node can be detected, for example, by an energy detector. Based on the observations $\hat{\phi}_i[j]$, for $i \in \mathcal{A}[j]$, the fusion node generates an MMSE estimate $\hat{\theta}[j]$ of $\theta[j]$.

III. MMSE ANALYSIS AND OPTIMIZATION

We now analyze the MSE of the estimate obtained by the fusion node. For this, we first characterize the steady state probability ζ that an EH sensor node is active in a slot. It has the following insightful closed-form.

Proposition 1: The steady state probability ζ that a sensor node is active in any slot is given by

$$\zeta = \min \left\{ \frac{P_{\text{eh}}}{(P + P_{\text{eh}})(1 - \tau)}, 1 \right\}. \quad (4)$$

Proof: The proof is relegated to Appendix A. ■

When $\zeta = 1$, we shall say that the node is *energy unconstrained*. Else, for $\zeta < 1$, we say that it is *energy constrained*.

A. Parameter Estimation at Fusion Node

The PLL-based receiver, which is shown in Fig. 2, comes up with an estimate $\hat{\Delta}_i[j]$ for the phase information $\Delta_i[j]$ in the signal received $y_i(t)$ from sensor node $i \in \mathcal{A}[j]$. As mentioned, $\hat{\phi}_i[j] = \hat{\Delta}_i[j] + 2\pi f_{c_i} \xi_i[j]$. Assuming the linearized model of a PLL [17, Chap. 5], as shown in Appendix B, $\hat{\phi}_i[j]$ equals

$$\hat{\phi}_i[j] = \theta_i[j] + w_i[j], \quad (5)$$

where $w_i[j] \sim \mathcal{N}\left(0, \sigma_m^2 + \frac{N_0 \Omega_{\text{eq}}}{2Ph_i^2[j]T(1-\tau)}\right)$ and is independent of $\theta_i[j]$, and $\Omega_{\text{eq}} = \int_0^\infty |H(\omega)|^2 d\omega$ is the effective noise bandwidth of the PLL.

The MMSE estimate $\hat{\theta}[j]$ given $h_i[j]$, for $i \in \mathcal{A}[j]$, can be written in terms of $\hat{\phi}_i[j]$ as [18, Chap. IV]

$$\hat{\theta}[j] = \frac{\sum_{i \in \mathcal{A}[j]} \hat{\phi}_i[j] \left(\sigma_m^2 + \frac{N_0 \Omega_{\text{eq}}}{2Ph_i^2[j]T(1-\tau)} \right)^{-1}}{\sum_{i \in \mathcal{A}[j]} \left(\sigma_m^2 + \frac{N_0 \Omega_{\text{eq}}}{2Ph_i^2[j]T(1-\tau)} \right)^{-1} + \frac{1}{\sigma_\theta^2}}. \quad (6)$$

Let $k = |\mathcal{A}[j]|$, where $|\cdot|$ denotes the cardinality of a set. By symmetry, the MSE $\epsilon(k)$ of $\hat{\theta}[j]$ averaged over $h_i[j]$, for $i \in \mathcal{A}[j]$, is a function of k . It is given by [18, Chap. IV]

$$\epsilon(k) = \mathbb{E} \left[\left(\sum_{i \in \mathcal{A}[j]} \left(\sigma_m^2 + \frac{N_0 \Omega_{\text{eq}}}{2Ph_i^2[j]T(1-\tau)} \right)^{-1} + \frac{1}{\sigma_\theta^2} \right)^{-1} \right]. \quad (7)$$

From (7), $2PT(1-\tau)/(N_0 \Omega_{\text{eq}})$ can be interpreted as SNR.

Lastly, the MSE χ of the estimate, averaged across the channel fades and the number of active sensor nodes, is

$$\chi = \sum_{k=0}^N \binom{N}{k} \zeta^k (1-\zeta)^{N-k} \epsilon(k). \quad (8)$$

The following result gives a closed-form formula for χ .

Result 1: The MSE χ of the estimate is given by

$$\chi \approx \sum_{k=0}^N \binom{N}{k} \zeta^k (1-\zeta)^{N-k} \sum_{\substack{l_1 \geq 0, \dots, l_M \geq 0 \\ \sum_{i=1}^M l_i = k}} \alpha_1^{l_1} \alpha_2^{l_2} \dots \alpha_M^{l_M} \times \left(\frac{1}{\sigma_\theta^2} + \sum_{i=1}^M \frac{\beta_i}{\sigma_m^2 \beta_i + \frac{N_0 \Omega_{\text{eq}}}{2PT(1-\tau)}} \right)^{-1}, \quad (9)$$

where α_i and β_i , for $i = 1, \dots, M$, are the weights and abscissas, respectively, of Gauss-Laguerre quadrature [19, Chap. 25], and ζ is given by (4).

Proof: The derivation is given in Appendix C. ■

We have found $M = 4$ terms to be sufficient to accurately compute χ for the parameters of interest.

B. Optimal τ and P

We now optimize τ and P to minimize the MSE. The following result shows that the optimal transmit power is P_{max} regardless of P_{eh} and τ .

Result 2: The optimal transmit power is P_{max} .

Proof: The proof is relegated to Appendix D. ■

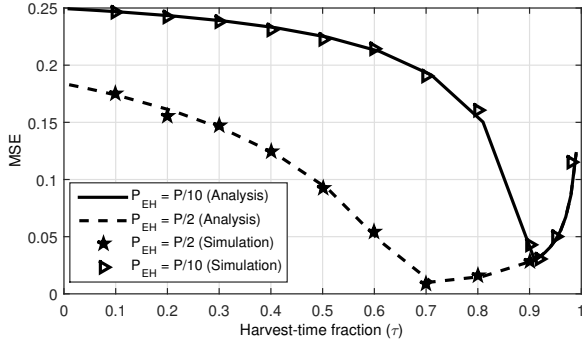


Fig. 3. MSE of estimate as a function of τ for different P_{ch}/P ($N = 1$ and $T = 100$ ms).

Thus, an RF EH sensor node should spend as less time on data transmission as possible by transmitting at peak power and maximize the time it spends on harvesting energy. It also leads to the following insightful lower bound on χ .

Result 3: The MSE χ is lower bounded as

$$\chi \geq \chi_{\text{lb}} = \left(\frac{N\zeta}{\sigma_m^2 + \frac{\Omega_{\text{eq}} N_0 (P_{\text{max}} + P_{\text{ch}})\zeta}{2P_{\text{max}}T}} + \frac{1}{\sigma_\theta^2} \right)^{-1}. \quad (10)$$

Proof: The proof is relegated to Appendix E. ■

It is difficult to analytically characterize the optimal τ that minimizes χ . However, significant insight can be gained by optimizing χ_{lb} . It can be shown that the optimal value of τ , denoted by τ_{opt} , that minimizes χ_{lb} in (10) is

$$\tau_{\text{opt}} = \frac{P_{\text{max}}}{P_{\text{max}} + P_{\text{ch}}}. \quad (11)$$

Comments: It can be shown that for $N = 1$, the optimal τ that minimizes χ is indeed τ_{opt} . It can also be shown that the difference between χ and χ_{lb} decreases as N increases. We, therefore, see that minimizing χ_{lb} yields the optimal τ for both small N and larger N .

Equation (11) implies that each sensor node should select the lowest value of τ that ensures that it is always active. Reducing τ below τ_{opt} makes it inactive with a non-zero probability, while increasing τ beyond τ_{opt} reduces the transmission time, both of which degrade the estimate at the fusion node.

IV. NUMERICAL RESULTS

We now present Monte Carlo simulations to study the trade-offs for different system parameter settings and assess the accuracy of our analysis. We set $\sigma_\theta = \pi/6$ and $\sigma_m = \pi/600$.

We use the following discrete-time implementation of the PLL-based receiver in our simulations [16]. The VCO generates a discrete-time sinusoid with phase equal to the cumulative sum of its input signal thus far. Thus, for the phase components, its transfer function is $\frac{1}{1-z^{-1}}$. The loop filter is an infinite impulse response (IIR) filter with transfer function $\kappa_p + \frac{\kappa_i}{1-z^{-1}}$. We choose $\kappa_p = 0.2$ and $\kappa_i = 0.1$. It can be shown that this choice ensures that the second-order PLL loop is stable [20].

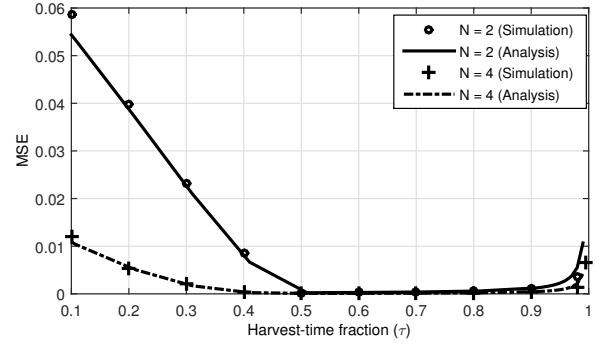


Fig. 4. MSE of estimate as a function of τ for different number of sensor nodes ($T = 100$ ms, $P_{\text{ch}} = P_{\text{max}}$).

Fig. 3 plots the MSE as a function of τ for different P_{ch}/P , with $P = P_{\text{max}}$. It brings out the trade-off associated with τ . As τ increases from 0, the MSE decreases because the probability that a sensor node transmits. This improves the quality of the estimate at the fusion node. However, for $\tau > \tau_{\text{opt}}$, the MSE increases because the smaller transmission time reduces the SNR. The optimal τ values for both $P_{\text{ch}} = P/10$ and $P_{\text{ch}} = P/2$ are in agreement with (11). The marginal mismatch between the analysis and simulation results is because of the linearized assumption in the PLL analysis. As P_{ch} decreases, the optimal τ increases to enable the sensor node to accumulate sufficient energy to transmit. When the optimal τ is close to 1, the MSE is very sensitive to τ .

Fig. 4 plots the MSE as a function of τ for different N . It again brings out the trade-off associated with τ , but as a function of number of nodes N . We see that as N increases, the MSE decreases considerably. This is because the net energy input to the system increases, since more nodes harvest energy. Furthermore, the number of observations increases and the spatial diversity in the system increases.

Benchmarking: Fig. 5 compares the MSEs of the analog scheme and digital schemes as a function of $2P_{\text{max}}T(1-\tau)/N_0$, which is the SNR scaled by Ω_{eq} . We set $N = 1$ and the transmission duration $T(1-\tau)$ as 100 ms. In the digital scheme, the sensor node quantizes its measurement using the MSE-optimal Lloyd-Max quantizer, which is designed for M quantization levels, and then transmits it to the fusion node using M-ary QAM. The receiver decodes the transmitted information and estimates the measurement. Both analog and digital schemes use the same bandwidth. The sensors are energy unconstrained in the regime under consideration. At low SNRs, the larger constellations fare worse due to their greater susceptibility to fading and noise, while the smaller constellations fare worse due to their larger quantization errors. Only when $2P_{\text{max}}T(1-\tau)/N_0 > 10$ dB, do 64-QAM and 256-QAM marginally outperform the analog scheme.

The figure brings out two advantages of the analog scheme. Firstly, in order to ensure a small MSE, the constellation size needs to be adjusted as a function of the SNR in the digital schemes. On the other hand, this is not required for the analog

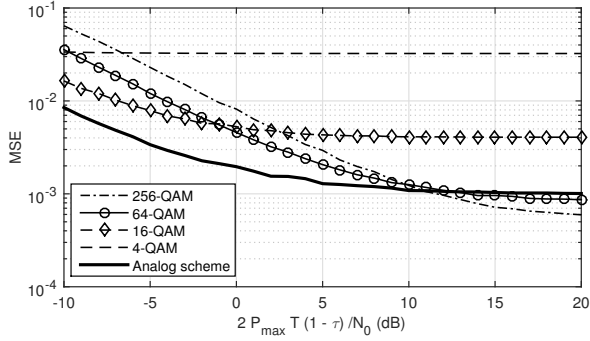


Fig. 5. Performance benchmarking: MSE of estimate as a function of $2P_{\max}T(1-\tau)/N_0$ for analog and digital transmission schemes ($N = 1$).

scheme. Secondly, constellation sizes as large as 64 or 256 are seldom used in WSNs due to their high peak-to-average-power ratios (PAPR), implementation complexity, and sensitivity to RF impairments. On the other hand, the analog scheme has a low PAPR and is easy to implement.

V. CONCLUSIONS

We highlighted the trade-offs involved in the design of an analog communication and estimation scheme in an RH EH WSN. For the time-sharing model, we analyzed and optimized the fading-averaged MSE of the estimate for a general class of stationary and ergodic RF EH processes. We saw that the analog scheme did not require a careful tuning of the quantizer and constellation size to the transmit power, which the digital schemes did. It also avoided the implementation difficulties associated with the digital schemes that used larger constellations. Future work involves evaluating the impact of imperfect channel estimates and incorrect detection by the fusion node of transmissions by the sensor nodes. Also, it is interesting to study the more general model in which the measurements of different nodes are correlated spatially.

APPENDIX

A. Proof of Prop. 1

In steady state, the average energy E_{out} used by a sensor node for transmissions is given by

$$E_{\text{out}} = \zeta PT(1-\tau). \quad (12)$$

The average energy input E_{in} into the sensor node consists of two terms: (i) the energy harvested in the harvesting duration, which equals $P_{\text{ch}}T\tau$, and (ii) the energy harvested in the data transmission duration if the battery lacks sufficient energy to transmit, which is given by $(1-\zeta)P_{\text{ch}}T(1-\tau)$. Thus,

$$E_{\text{in}} = P_{\text{ch}}T\tau + (1-\zeta)P_{\text{ch}}T(1-\tau). \quad (13)$$

Consider first the case where $\zeta < 1$. This occurs only if $E_{\text{in}} = E_{\text{out}}$. Equating (12) and (13) and rearranging, we get $\zeta = \frac{P_{\text{ch}}}{(P+P_{\text{ch}})(1-\tau)}$. The other alternative is $\zeta = 1$, which means that the EH sensor node always has enough energy to transmit. This happens when $E_{\text{in}} \geq E_{\text{out}}$, which implies that $\frac{P_{\text{ch}}}{(P+P_{\text{ch}})(1-\tau)} \geq 1$. Combining these yields (4).

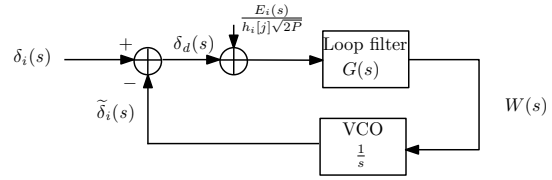


Fig. 6. Linearized PLL model in transform domain.

B. Derivation of (5)

Using the linearized PLL model, we first characterize the statistics of the noise in $\tilde{\Delta}_i(t)$, along lines similar to [17, Chap. 5]. Fig. 6 shows the Laplace transform-domain representation of the phase components of the signals in the model. Let $E_i(s)$, $W(s)$, $\tilde{\delta}_i(s)$, $\delta_i(s)$ and $\delta_d(s)$ denote the transforms of $e_i(t)$, $w(t)$, $\tilde{\Delta}_i(t)$, $\Delta_i[j]$ and $\Delta_d(t)$, respectively, defined over the support $(j-1)T + \tau T \leq t < jT$. The noise component $E_i(s)$ in the received signal is replaced by an equivalent noise $E_i(s)/(h_i[j]\sqrt{2P})$ generated within the PLL loop.

Since the VCO generates a signal whose phase is the integral of its input signal, its transfer function is $1/s$. Since $e_i(t)$ is a Gaussian random process, the noise $\tilde{z}_i(t)$ in $\tilde{\Delta}_i(t)$ is also Gaussian random process. Thus, for $(j-1)T + \tau T \leq t < jT$,

$$\tilde{\Delta}_i(t) = \Delta_i[j] + \tilde{z}_i(t), \quad (14)$$

where $\mathbb{E}[\tilde{z}_i^2(t)] = \frac{\mathbb{E}[e_i^2(t)]\Omega_{\text{eq}}}{h_i[j]^2 P} = \frac{N_0\Omega_{\text{eq}}}{2h_i^2[j]P}$. Since $H(s)$ is a second-order transfer function, the steady state phase error in a slot between $\tilde{\Delta}_i(t)$ and $\Delta_i[j]$ is 0 for a step-wise change in input phase $\tilde{\Delta}_i[j]$. Thus, $\mathbb{E}[\tilde{z}_i(t)] = 0$.

Averaging $\tilde{\Delta}_i(t)$ in (14) over the transmission duration $T(1-\tau)$, the noise-averaged phase estimate $\hat{\Delta}_i[j]$ is

$$\hat{\Delta}_i[j] = \Delta_i[j] + z_i[j], \quad (15)$$

where $z_i[j] = \int_{(j-1)T+\tau T}^{jT} \tilde{z}_i(v)dv/(T(1-\tau)) \sim \mathcal{N}(0, \sigma_{z_i}^2[j])$ and $\sigma_{z_i}^2[j] = N_0\Omega_{\text{eq}}/(2h_i^2[j]PT(1-\tau))$. Subtracting $2\pi f_{c_i}\xi_i[j]$ from both sides of (5) and substituting (1) in (5), we get $\phi_i[j] = \theta[j] + w_i[j]$, where $w_i[j] = n_i[j] + z_i[j]$. Since $n_i[j]$ and $z_i[j]$ are mutually independent, it follows that $w_i[j] \sim \mathcal{N}(0, \sigma_m^2 + \frac{N_0\Omega_{\text{eq}}}{2h_i^2[j]PT(1-\tau)})$. It can also be shown that $\theta[j]$ and $w_i[j]$ are mutually independent.

C. Brief Derivation of Result 1

Let $X_i[j] = \frac{h_i^2[j]}{h_i^2[j]\sigma_m^2 + \frac{N_0\Omega_{\text{eq}}}{2PT(1-\tau)}}$. Since $h_i^2[j]$ is an exponential RV with unit mean, it can be shown that the probability density function $f_{X_i[j]}(x)$ of $X_i[j]$ is given by

$$f_{X_i[j]}(x) = \begin{cases} \frac{N_0\Omega_{\text{eq}}e^{-\frac{N_0\Omega_{\text{eq}}x}{2PT(1-\tau)(1-\sigma_m^2x)}}}{2PT(1-\tau)(1-\sigma_m^2x)^2}, & \text{if } x \in [0, \sigma_m^{-2}], \\ 0, & \text{else.} \end{cases} \quad (16)$$

Thus, its moment generating function (MGF) $\Psi_{X_i[j]}(s)$ is

$$\Psi_{X_i[j]}(s) = \int_0^{\frac{1}{\sigma_m^2}} \frac{N_0\Omega_{\text{eq}}e^{-sx}e^{-\frac{N_0\Omega_{\text{eq}}x}{2PT(1-\tau)(1-\sigma_m^2x)}}}{2PT(1-\tau)(1-\sigma_m^2x)^2} dx. \quad (17)$$

Substituting $q = \frac{N_0\Omega_{\text{eq}}}{2PT(1-\tau)} \frac{x}{(1-\sigma_m^2 x)}$ in (17) yields

$$\Psi_{X_i[j]}(s) = \int_0^\infty e^{-\frac{sq}{\sigma_m^2 q + \frac{N_0\Omega_{\text{eq}}}{2PT(1-\tau)}}} e^{-q} dq. \quad (18)$$

Let $Y = \sum_{i \in \mathcal{A}[j]} X_i[j] + \frac{1}{\sigma_\theta^2} > 0$. From (18), its MGF is given by $\Psi_Y(s) = \left(\int_0^\infty e^{-\frac{sq}{\sigma_m^2 q + \frac{N_0\Omega_{\text{eq}}}{2PT(1-\tau)}}} e^{-q} dq \right)^k e^{-\frac{s}{\sigma_\theta^2}}$. The MSE $\epsilon(k)$ is given by $\epsilon(k) = \mathbb{E}[Y^{-1}] = \int_0^\infty \Psi_Y(s) ds$. Thus,

$$\epsilon(k) = \int_0^\infty \left(\int_0^\infty e^{-\frac{sq}{\sigma_m^2 q + \frac{N_0\Omega_{\text{eq}}}{2PT(1-\tau)}}} e^{-q} dq \right)^k e^{-\frac{s}{\sigma_\theta^2}} ds. \quad (19)$$

Expanding the integral using Gauss-Laguerre quadrature, using the multinomial theorem, and simplifying further, we get

$$\epsilon(k) \approx \sum_{\substack{l_1 \geq 0, \dots, l_M \geq 0 \\ \sum_{i=1}^M l_i = k}} \frac{\binom{k}{l_1, \dots, l_M} \alpha_1^{l_1} \dots \alpha_M^{l_M}}{\left(\frac{1}{\sigma_\theta^2} + \sum_{i=1}^M \frac{\beta_i}{\sigma_m^2 \beta_i + \frac{N_0\Omega_{\text{eq}}}{2PT(1-\tau)}} \right)}. \quad (20)$$

Substituting (20) in (8) yields Result 1.

D. Proof of Result 2

Let the pair (τ, P) be called an *operating point* of the system. Clearly, the set of operating points lies within the region $0 \leq \tau \leq 1$ and $0 \leq P \leq P_{\max}$. Let \mathcal{U} denote the locus of all operating points that satisfy $\frac{P_{\text{ch}}}{(P_{\text{ch}}+P)(1-\tau)} = 1$. The following claims imply that the optimal power is P_{\max} .

Claim 1: Operating points that lie above \mathcal{U} are suboptimal.

Proof: For an operating point that lies above \mathcal{U} , it follows from Prop. 1 that $\zeta = 1$. Hence, from (8), the MSE equals

$$\chi = \mathbb{E} \left[\left(\sum_{i \in \mathcal{A}[j]} \left(\sigma_m^2 + \frac{N_0\Omega_{\text{eq}}}{2Ph_i^2[j]T(1-\tau)} \right)^{-1} + \frac{1}{\sigma_\theta^2} \right)^{-1} \right]. \quad (21)$$

From (21), it is clear that keeping P fixed and increasing τ reduces the MSE χ . ■

Claim 2: Any operating point on \mathcal{U} with $P < P_{\max}$ is suboptimal.

Proof: For an operating point that lies on \mathcal{U} , we have $\zeta = 1$. Therefore, the MSE is again given by (21). As we traverse \mathcal{U} , as τ increases, $P(1-\tau)$ also increases so as to keep $\frac{P_{\text{ch}}}{(P_{\text{ch}}+P)(1-\tau)}$ constant. Since $P(1-\tau)$ increases, it follows from (21) that the MSE decreases. ■

Claim 3: All operating points with $P < P_{\max}$ that lie below \mathcal{U} are suboptimal.

Proof: For such an operating point, from Prop. 1, we know that $\zeta < 1$. Let us increase P such that ζ remains constant. From (7), $\epsilon(k)$ decreases. Therefore, from (8), it follows that the MSE χ decreases. ■

E. Brief Proof of Result 3

Substituting $P = P_{\max}$ and the expression for ζ from (4) in (8), it can be shown that the function inside $\mathbb{E}[\cdot]$ in (7) is a

convex function of $h_i[j]$, for $i \in \mathcal{A}[j]$. Applying the Jensen's inequality, we get

$$\chi > \sum_{k=0}^N \frac{\binom{N}{k} \zeta^k (1-\zeta)^{N-k}}{\sigma_m^2 + \frac{N_0\Omega_{\text{eq}}(P_{\text{ch}}+P_{\max})\zeta}{2P_{\max}P_{\text{ch}}T\mathbb{E}[h_i^2[j]]} + \frac{1}{\sigma_\theta^2}}, \quad (22)$$

$$= \mathbb{E} \left[\left(\frac{K}{\sigma_m^2 + \frac{N_0\Omega_{\text{eq}}(P_{\text{ch}}+P_{\max})\zeta}{2P_{\max}P_{\text{ch}}T}} + \frac{1}{\sigma_\theta^2} \right)^{-1} \right], \quad (23)$$

where the last expectation is over K , which is a binomial RV with mean $\mathbb{E}[K] = N\zeta$. Applying the Jensen's inequality to the discrete RV K yields (10).

REFERENCES

- [1] Y. Zhao, B. Chen, and R. Zhang, "Optimal power allocation for an energy harvesting estimation system," in *Proc. IEEE ICASSP*, May 2013, pp. 4549–4553.
- [2] C. Huang, Y. Zhou, T. Jiang, P. Zhang, and S. Cui, "Power allocation for joint estimation with energy harvesting constraints," in *Proc. IEEE ICASSP*, May 2013, pp. 4804–4808.
- [3] M. Nourian, S. Dey, and A. Ahlen, "Distortion minimization in multi-sensor estimation with energy harvesting," *IEEE J. Select. Areas Commun.*, vol. 33, no. 3, pp. 524–539, Mar. 2015.
- [4] Y. Hong and P. Win, "Distributed estimation with analog forwarding in energy-harvesting wireless sensor networks," in *Proc. IEEE ICCS*, Nov. 2014, pp. 142–146.
- [5] S. Rao and N. B. Mehta, "Energy harvesting WSNs for accurately estimating the maximum sensor reading: Trade-offs and optimal design," *IEEE Trans. Wireless Commun.*, vol. 15, no. 8, pp. 4562–4573, Aug. 2015.
- [6] H. J. Visser, A. C. F. Reniers, and J. A. C. Theeuwes, "Ambient RF energy scavenging: GSM and WLAN power density measurements," in *Proc. 38th Eur. Microw. Conf.*, Oct. 2008, pp. 721–724.
- [7] L. Liu, R. Zhang, and K.-C. Chua, "Multi-antenna wireless powered communication with energy beamforming," *IEEE Trans. Commun.*, vol. 62, no. 12, pp. 4349–4361, Dec. 2014.
- [8] H. Jabbar, Y. S. Song, and T. T. Jeong, "RF energy harvesting system and circuits for charging of mobile devices," *IEEE Trans. Consum. Electron.*, vol. 56, no. 1, pp. 247–253, Feb. 2010.
- [9] R. Zhang and C. K. Ho, "MIMO broadcasting for simultaneous wireless information and power transfer," *IEEE Trans. Wireless Commun.*, vol. 12, no. 5, pp. 1989–2001, May 2013.
- [10] K. Huang and E. Larsson, "Simultaneous information and power transfer for broadband wireless systems," *IEEE Trans. Signal Proc.*, vol. 61, no. 23, pp. 5972–5986, Dec. 2013.
- [11] L. Xiao, P. Wang, D. Niyato, D. Kim, and Z. Han, "Wireless networks with RF energy harvesting: A contemporary survey," *IEEE Commun. Surveys Tuts.*, vol. 17, no. 2, pp. 757–789, Second quarter 2015.
- [12] J. Li and G. AlRegib, "Network lifetime maximization for estimation in multihop wireless sensor networks," *IEEE Trans. Signal Proc.*, vol. 57, no. 7, pp. 2456–2466, Jul. 2009.
- [13] M. Gastpar and M. Vetterli, "Source-channel communication in sensor networks," in *Lecture Notes in Comput. Sci.* New York: Springer, Apr. 2003, pp. 162–177.
- [14] A. Seyedi and B. Sikdar, "Energy efficient transmission strategies for body sensor networks with energy harvesting," *IEEE Trans. Commun.*, vol. 58, no. 7, pp. 2116–2126, Jul. 2010.
- [15] S. Cui, J. Xiao, A. J. Goldsmith, Z.-Q. Luo, and H. V. Poor, "Estimation diversity and energy efficiency in distributed sensing," *IEEE Trans. Signal Process.*, vol. 55, no. 9, pp. 4683–4695, Sep. 2007.
- [16] W. Li and J. Meiners, "Introduction to phase-locked loop system modeling," *Texas Instruments Inc. J. Analog Appl.*, pp. 5–10, May 2000.
- [17] J. G. Proakis and M. Salehi, *Digital Communications*, 5th ed. McGraw Hill, 2007.
- [18] H. V. Poor, *An Introduction to Signal Detection and Estimation*, 2nd ed. Springer-Verlag, Inc., 1994.
- [19] M. Abramowitz and I. Stegun, *Handbook of mathematical functions*. Dover Publications, 1970.
- [20] K. Ogata, *Discrete-time Control Systems*, 2nd ed. Prentice-Hall International, Inc., 1995.